RSC Advances

PAPER

View Article Online
View Journal | View Issue

Check for updates

Cite this: *RSC Adv.*, 2026, **16**, 16694

Enhanced ammonia sensing using Pt-decorated single-crystalline SnO_2 nanowires prepared by sputtering

Nguyen Phu Hung, Tran Nguyen Anh Quan, Luu Trung Tien, Nguyen Van Duy,* Chu Thi Xuan, Tran Thi Viet Nga, Dang Thi Thanh Le, Chu Manh Hung and Nguyen Duc Hoa *

Received 9th January 2026
Accepted 5th March 2026

DOI: 10.1039/d6ra00229c

rsc.li/rsc-advances

Ammonia is a well-known toxic and colorless gas that is widely produced in various chemical and biological industries; thus, developing high-performance gas sensors for the detection of NH_3 is essential. Herein, we prepared a high-performance NH_3 gas sensor based on SnO_2 nanowires coated with Pt by the sputtering method and studied the effect of Pt coating on the gas-sensing performance. Single-crystal SnO_2 nanowires were grown by the CVD method, and sputtering was used to control the thickness of the Pt coating layer. We demonstrated that the NH_3 gas-sensing performance of Pt–SnO_2 nanowires was significantly enhanced compared to that of pristine SnO_2 nanowires. The 5 nm Pt–SnO_2 nanowire sensor exhibits a high response (R_a/R_g) of 19.98 toward 500 ppm NH_3 gas, which is a 19-fold enhancement compared with that of the bare SnO_2 nanowires. The sensor exhibited a fast response and recovery with excellent selectivity over the interfering species C_2H_4, H_2, and acetone. We also proposed a mechanism for the enhanced sensitivity of Pt–SnO_2 nanowires toward NH_3.

Open Access Article. Published on 26 March 2026. Downloaded on 4/7/2026 11:06:58 PM.
This article is licensed under a Creative Commons Attribution-NonCommercial 3.0 Unported Licence.

1. Introduction

Gas sensors, which can detect or measure trace amounts of toxic and/or explosive gases, have attracted considerable attention from researchers worldwide because of their broad potential applications in air pollution monitoring, healthcare, military, and automotive systems.[1–3] Especially, the need to monitor hazardous gases, including CO, CO_2, NO_2, SO_2, H_2S, and NH_3, has been increasing with rising concerns about the environment and human health. Among these hazardous gases, ammonia (NH_3) is highly toxic even at low concentrations (*e.g.*, ppm levels).[4,5] Exposure to 400 ppm NH_3 for one hour may cause throat irritation, whereas concentrations as low as 25 ppm can be readily detected by odor. Accordingly, OSHA has set the permissible limit for NH_3 exposure at 50 ppm for an 8 hour workday. Therefore, real-time monitoring of NH_3 at low concentrations, at ppm levels, is vital for applications in air pollution control and food quality monitoring.[6]

Nowadays, gas detection tools include infrared absorbers, ion mobility spectrometers, and gas chromatographs. However, these methods have the disadvantages of being time-consuming with complicated operations and high costs, which make it difficult to meet the growing demands.[7,8] Therefore, the development of next-generation toxic and harmful gas detection techniques is imperative to protect humans from potential health risks.[2] Resistive gas sensors based on metal-oxide semiconductors were reported to exhibit significant advantages, including a simple device structure, compatibility with silicon technology and suitability for miniaturized platforms, making them ideally suitable for real-time monitoring and early warning of NH_3 leakage.[9] For these reasons, the exploration and development of high-performance gas sensors have attracted widespread attention from scientists in recent years.[4]

In recent studies, different materials have been synthesized for gas sensor applications.[10–12] Metal-oxide semiconductor-based gas sensors (MOS) have attracted significant attention for NH_3 detection, especially SnO_2, ZnO, WO_3, and TiO_2.[13,14] MOS can be classified into n-type or p-type semiconductors depending on the deficiency or excess of oxygen in their composition, which consequently determines their gas-sensing properties. An increased density of active sites on the surface of the sensing material is expected to enhance sensor sensitivity.[14,15] The intrinsic properties of metal oxides, namely, low cost, thermal stability, nontoxicity, and high chemical sensitivity, are ascribed effectively for a chemiresistive gas sensor. Furthermore, the mechanism of gas sensors mostly depends on the size of metal-oxide particles and their crystallinity.[15] Ultraviolet or visible light irradiation was also used to enhance the gas-sensing performance of pure metal oxides and CdS/WSe_2/CdS heterojunction.[16,17] Tin oxide (SnO_2), an n-type semiconductor with an energy gap of 3.6 eV, is one of the most widely used oxides for developing toxic gas detectors.[18] The applications of SnO_2 for gas sensing have also

School of Materials Science and Engineering, Hanoi University of Science and Technology, No 1 Dai Co Viet, Hanoi, Vietnam. E-mail: duy.nguyenvan@hust.edu.vn; ndhoa@itims.edu.vn

© 2026 The Author(s). Published by the Royal Society of Chemistry

Open Access Article. Published on 26 March 2026. Downloaded on 4/7/2026 11:06:58 PM. This article is licensed under a Creative Commons Attribution-NonCommercial 3.0 Unported Licence.

attracted considerable attention due to its excellent gas response. The introduction of noble metal nanostructures (Pd, Pt, Ag, Cu, and Ni) is considered an effective way to enhance the gas response as well as lower the operating temperature of the sensor.[18] The enhancement of the sensitivity of the metal-oxide gas sensor by surface decoration with noble metal nanoparticles was ascribed to the formation of a heterojunction at the metal-oxide interface, and the catalytic activity of noble metal nanoparticles.[18,19] For metal oxide-based gas sensors, room-temperature and low-temperature sensors have attracted great interest due to their low power consumption.[19,20] Noble functionalization on metal oxides can also reduce the operating temperature of gas sensors.[21,22] However, effective control of the decoration of noble metal nanoparticles on the surface of nanomaterials for enhanced gas-sensing performance is still a challenge.

Herein, Pt–SnO_2 nanowire NH_3 sensors were fabricated by chemical vapor deposition combined with sputtering modification of Pt nanoparticles. We precisely controlled Pt deposition to optimize gas-sensing performance. Experiments showed that the Pt-decorated-SnO_2 (PS) sensors have high sensing response and short response/recovery as compared with pristine SnO_2 nanowires. Furthermore, the sensing mechanism of PS was studied and investigated. Our results indicate that the PS-based sensor exhibits a 19-fold higher performance than pure SnO_2 under the same experimental conditions. Additionally, the sensors exhibited excellent selectivity for ammonia over contaminants, such as ethylene and acetone.

2. Experimental

2.1 Materials

In the experimental process, the analytical substance consisting of pure tin powder (99.99% Sn) was used for the growth of SnO_2 nanowires, whereas a two-inch Pt (99.99%) target was used for the deposition of a Pt catalyst layer. The experimental process includes two main stages: (i) chemical vapor deposition (CVD) growth of SnO_2 nanowires and (ii) sputtering deposition of Pt nanoparticles, as shown in Fig. 1.

2.2 Preparation of SnO_2 nanowires

The preparation of SnO_2 nanowire gas sensors has been described in our previous articles as published elsewhere.[23] As reported, the SnO_2 nanowires were synthesized by a chemical vapor deposition (CVD) method using a lab-made system, where we studied the effect of growth temperature and growth time on the density and morphology of the nanowires. In this work, to ensure the growth of SnO_2 nanowires on a glass substrate without melting it, we used a low temperature of 730 °C with a growth time of 8 min. In a typical procedure, SnO_2 nanowires were grown at 730 °C with pure Sn powder as an evaporation source. The evaporation source and Pt interdigital electrodes were loaded at the center zone of the CVD system, and the temperature was increased to 730 °C within 30 min. The SnO_2 nanowire growth process was carried out for 8 min with a flow rate of 0.5 sccm oxygen, introduced evenly into the reaction chamber, and a pressure of about 10^{-1} Torr. After the completion of the growth process of SnO_2 nanowires, the furnace was cooled down naturally to room temperature (RT).

2.3 Decoration of Pt nanoparticles

The Pt decorated SnO_2 nanowires were prepared using the sputtering method. Briefly, a 50 W DC power source was used to bombard the Pt target in a plasma-containing environment, ejecting atoms from the target. Then, these ejected atoms were deposited on the surface of SnO_2 nanowires. In this process, the density of Pt nanoparticles decorated on the surface of SnO_2 nanowires was controlled by varying the sputtering time. The samples were denoted as PS-30, PS-50, and PS-75 corresponding to the sputtering times of 30 s, 50 s, and 75 s, respectively (Table 1). The Pt thickness was measured on a thin film sample deposited on a Si wafer using a stylus profilometer (Dektak Pro, Bruker, Germany). The morphology, composition, structure, and gas-sensing properties of the Pt-decorated SnO_2 materials

Table 1 Samples at different sputtering times

Sample	Sputtering time (seconds)	Pt thickness (nm)
SnO_2 NWs	None	None
PS-30	30 s	3 nm
PS-50	50 s	5 nm
PS-75	75 s	8 nm

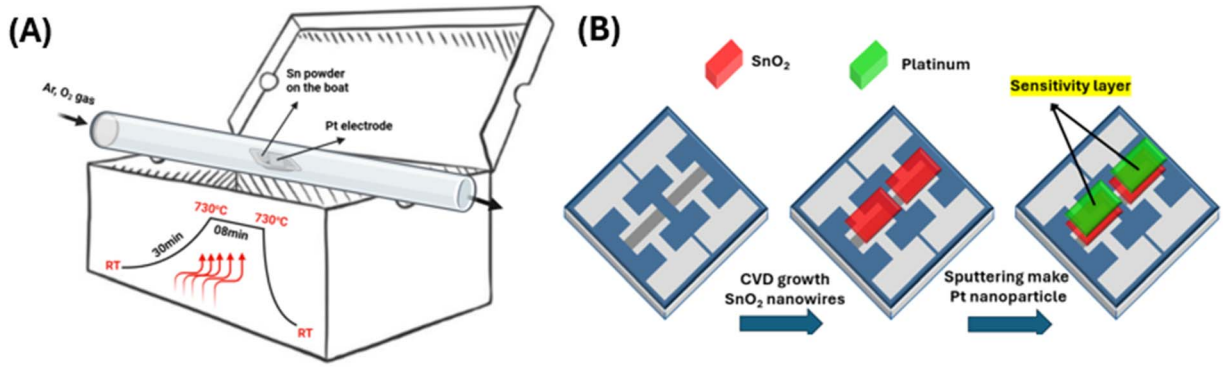

Fig. 1 Schematic of the (A) synthesis of SnO_2 nanowires and (B) decoration of Pt nanoparticles.

Open Access Article. Published on 26 March 2026. Downloaded on 4/7/2026 11:06:58 PM.
This article is licensed under a Creative Commons Attribution-NonCommercial 3.0 Unported Licence.

were investigated by scanning electron microscopy (SEM; JEOL 7600F), energy-dispersive X-ray spectroscopy (EDS), high-resolution transmission electron microscopy (HRTEM, JEOL, JEM-2100), selective area electron diffraction (SAED), and a gas-sensing system based on the change in resistance.[23] The electrical properties and gas-sensing characteristics of the fabricated sensors were studied by using a homemade gas-sensing measurement system, as reported in ref. 24. Briefly, the sensor was placed on a hot plate with controlled temperature ranging from 250 to 450 °C, while its electrical properties were measured. The electrical properties were studied by current–voltage (I–V) measurements under a bias voltage of ±5 V. The sensor resistance was monitored while exposing the devices to NH_3 with different concentrations at various temperatures. The sensor response was defined as the resistance ratio of the sensor in air (R_a) to that in the target gas (R_g). The response time and recovery time are defined as the time required for the sensor signal to reach 90% of the total change after exposure to the target gas (response) and after removal of the target gas (recovery), respectively.[25]

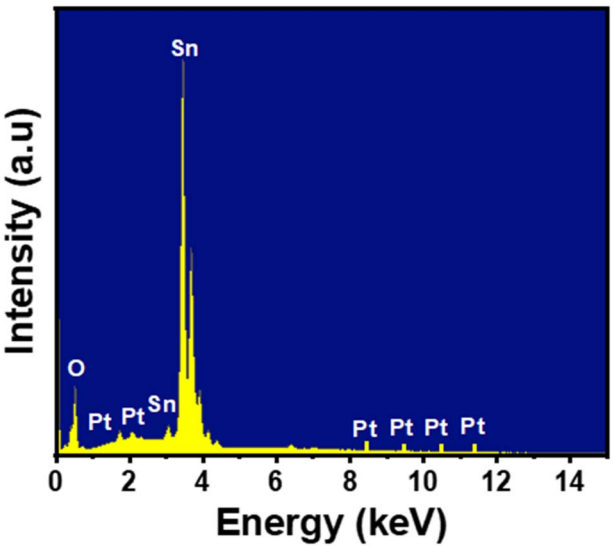

Fig. 3 EDS spectrum of the PS-50 sensor.

3. Results and discussion

3.1 Characterization of materials

To investigate the influence of the synthesis process on the morphologies, crystal structures and gas-sensing properties of SnO_2 nanowires and Pt/SnO_2 nanowires, we compared their SEM, EDS, HRTEM, SAED, I–V curves, and NH_3 gas response, as shown below.

The SEM images of SnO_2 and Pt-decorated SnO_2 samples are shown in Fig. 2, confirming the successful growth of nanowires on the entire Pt electrodes. As shown in Fig. 2(A1 and C1), the SnO_2 nanowires have an average length of about 8 micrometers, whereas the average diameter is about 80 nm. The nanowires grew on the surface of the Pt electrodes, but none of the nanowires grew on the bare SiO_2 substrate due to the catalytic activity of the Pt electrode. The size distribution histograms of SnO_2 nanowires and Pt–SnO_2 nanowires are shown in the insets in Fig. 2(C1 and C2), respectively. It is clear that the nanowires have diameters ranging from 50 to 200 nm, suggesting the growth process was not entirely uniform. The number of nanowires with small diameters of about 50–100 nm is higher than others. Pt was decorated on the surface of SnO_2 nanowires by the sputtering method, as shown in Fig. 2(A2 and C2). There was a slight difference in the morphology of the sample after the deposition of Pt nanoparticles. However, we could not observe the individual Pt nanoparticle in the SEM images because of the limited resolution.

As the SEM images did not provide clear evidence of Pt nanoparticles on the surface of the SnO_2 nanowires, we used the EDS analysis to determine the composition of the PS-50 sensor, as shown in Fig. 3. The EDS spectrum acquired at 15 keV displays the presence of Sn, O and Pt elements with weight

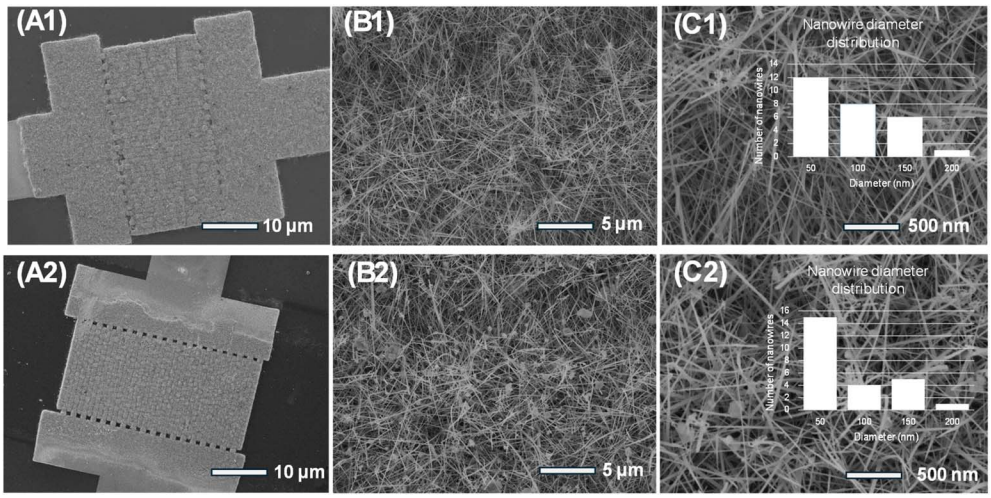

Fig. 2 SEM images of sensors with different magnifications: (A1) and (C1) SnO_2 nanowires and (A2) and (C2) Pt-decorated SnO_2 nanowires. Insets in (C1) and (C2) show the corresponding nanowire-diameter distributions.

© 2026 The Author(s). Published by the Royal Society of Chemistry

Open Access Article. Published on 26 March 2026. Downloaded on 4/7/2026 11:06:58 PM.
This article is licensed under a Creative Commons Attribution-NonCommercial 3.0 Unported Licence.

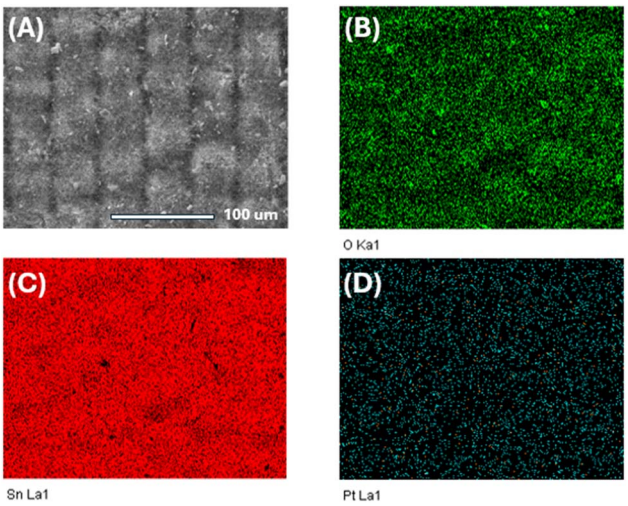

Fig. 4 (A) SEM image of PS-50 and the elemental mappings for (B) O, (C) Sn, and (D) Pt elements in the sensor.

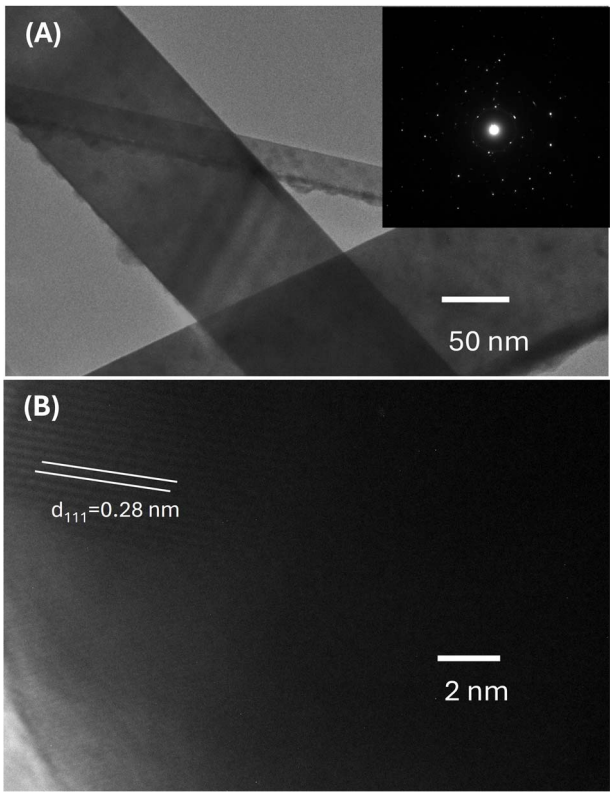

Fig. 5 (A) TEM and (B) HRTEM images of the Pt–SnO_2 nanowires.

percentages of 28.29 wt%, 70.26 wt% and 1.45 wt%, respectively. Therefore, the EDS results further verify the successful fabrication of the PS-50 sample with Pt decoration on the surface of SnO_2 nanowires.

Additionally, elemental mapping was performed to evaluate the elemental distribution in the PS-50 sample, as shown in Fig. 4A–D. The EDS mapping data confirm the uniform distribution of O, Sn, and Pt elements over the entire surface of the sample, indicating the effective decoration of Pt on the surface of SnO_2 nanowires. Furthermore, the Pt content is significantly lower than that of Sn and O due to the short sputtering time (50 s).

The microstructure and crystallinity of Pt–SnO_2 nanowires investigated by HRTEM images are shown in Fig. 5. The diameter of the large nanowire is about 80 nm, whereas the small nanowire is about 50 nm (Fig. 5A). We could observe many tiny Pt nanoparticles of about 5–10 nm in size decorated on the surface of the nanowires. By counting the number of Pt nanoparticles and their average size, we estimated that the density of Pt nanoparticles is about 500 particles per μm^2 surface of SnO_2 nanowires. The SEAD pattern (inset of Fig. 5A) exhibits sharp diffraction spots, confirming the single crystallinity of SnO_2 nanowires. The HRTEM image (Fig. 5B) shows lattice fringes with interplanar spacing matching well with Pt crystalline planes, particularly the Pt (111) plane (0.28 nm). The result is in good agreement with a recent report.[26] The HRTEM observation and SEAD analysis confirm the successful decoration of Pt nanoparticles on the surface of single-crystal SnO_2 nanowires.

3.1.1 Electrical and gas-sensing properties. The electrical properties of the fabricated sensors were investigated by measuring their *I–V* characteristics at 250–450 °C using a source meter (Keithley 2602). At each temperature, the *I–V* characteristics were measured in air for 100 data points within a bias range of ±5 V with a 0.3 s interval between observations.[23]

The *I–V* plots of the SnO_2 nanowires and PS-30, PS-50, and PS-75 sensors are shown in Fig. 6A–D respectively, indicating the linear dependence of current (*I*) on applied voltage (*V*), which is regarded as Ohmic contact between the Pt electrode and the sensing materials. Herein, the Ohmic behavior at the Pt/SnO_2 interface can be attributed to the direct growth of SnO_2 nanowires on Pt, which ensures clean contact with low interfacial resistance, as well as to the high carrier concentration induced by oxygen vacancies, which enables electron tunneling across the thin depletion region. An Ohmic contact in resistive gas sensors ensures that the device response is dominated by the surface sensing mechanism instead of interfacial contact effects.[27]

In this study, the as-prepared sensors with different sputtering times of Pt (30 s, 50 s, and 75 s) were tested toward NH_3 gas under dynamic conditions. NH_3 concentrations ranging from 25 to 500 ppm were tested at various working temperatures. Prior to the measurements, the sensors were stabilized on a hot plate with an air flow rate of 400 sccm for 1 h until a stable resistance was achieved. Once the resistance reached a steady state, NH_3 was introduced into the measurement chamber by switching the gas valve for 200 seconds per pulse. The sensor was then allowed to recover to its baseline resistance under an air flow of 400 sccm.[24] Moreover, it is crucial to figure out the optimal sensor and investigate their gas-sensing characteristics. Three different types of sensors corresponding to different sputtering times of Pt nanoparticles, namely, PS-30, PS-50, and PS-75, were tested, and we found that the PS-50 sensor demonstrated a superior response towards NH_3 as compared to the others (data not shown).

Open Access Article. Published on 26 March 2026. Downloaded on 4/7/2026 11:06:58 PM.
This article is licensed under a Creative Commons Attribution-NonCommercial 3.0 Unported Licence.

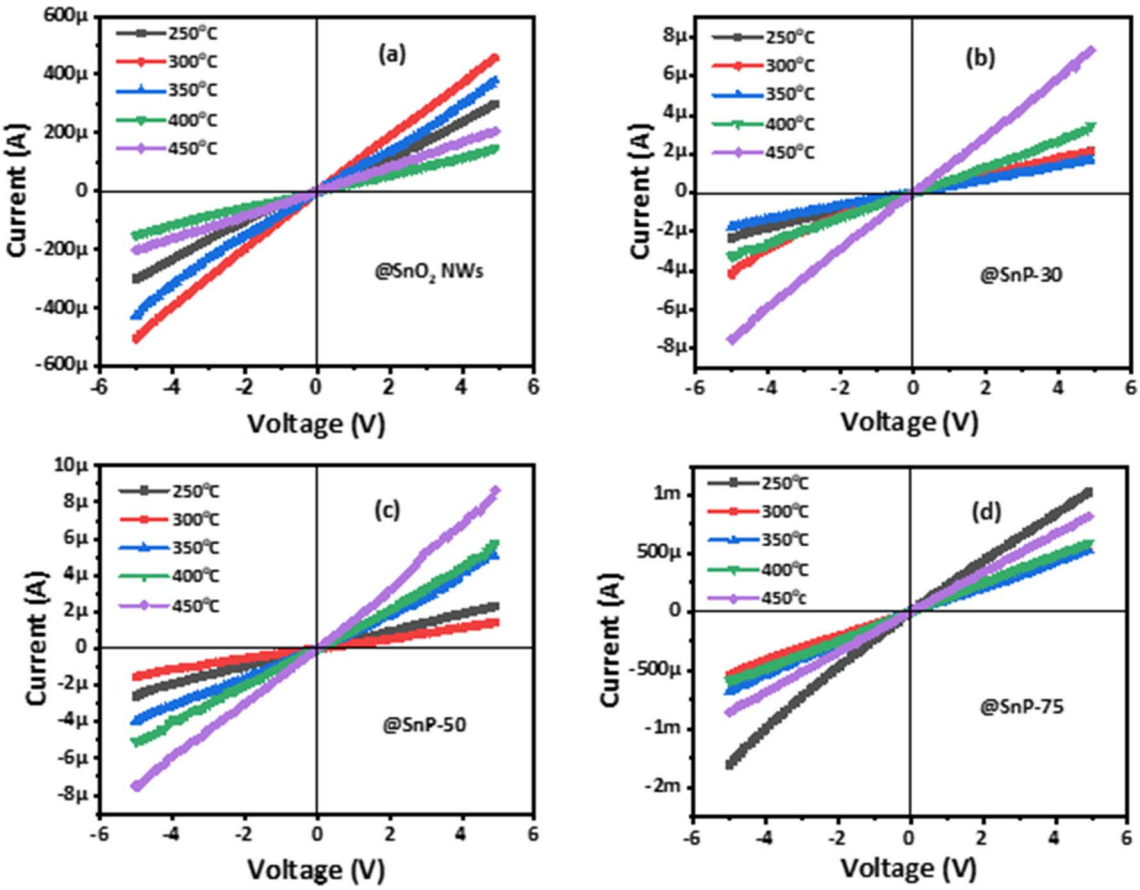

Fig. 6 The current–voltage characteristics of (a) SnO_2 nanowires, (b) PS-30, (c) PS-50 and (d) PS-75 sensors measured in the range of 250–450 °C in air.

As depicted in Fig. 7A, PS-50 was exposed to increasing concentrations of NH_3 gas at different operating temperatures. Notably, PS-50 demonstrated a fast response and recovery towards 500 ppm NH_3 with response/recovery times of 6/9 seconds at 450 °C. However, the response and recovery times of the sensor show an upward trend as the operating temperature decreases. The phenomenon occurred due to the activity of oxygen ions adsorbed on the surface of the material and the gas adsorption and desorption mechanism. The increase in response and recovery times at lower operating temperatures can be attributed to slower surface reaction kinetics and reduced desorption rates of reaction products. Fig. 7B displays the sensor response as a function of NH_3 concentration at 250–450 °C. The response increases with increasing NH_3

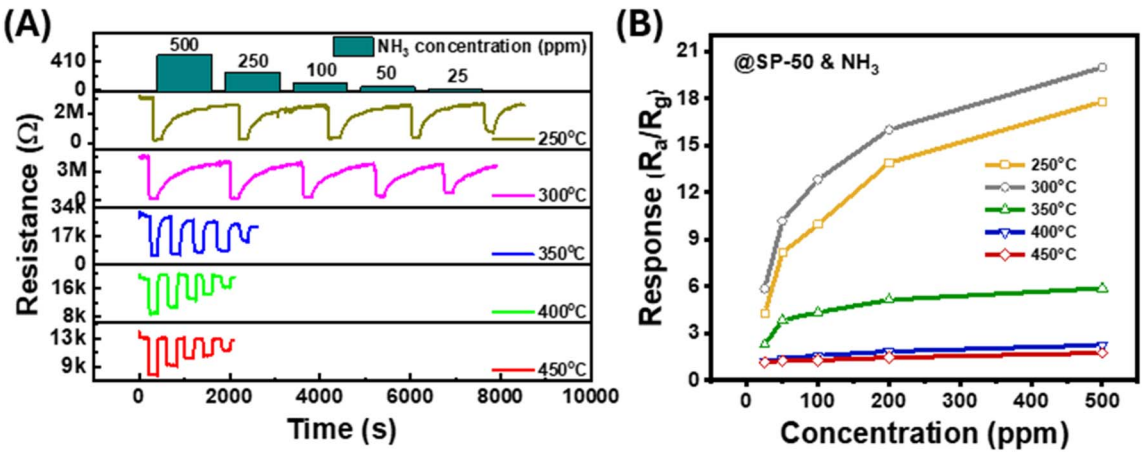

Fig. 7 (A) Resistance of the PS-50 sensor at various working temperatures and (B) sensor response as a function of the NH_3 concentration.

© 2026 The Author(s). Published by the Royal Society of Chemistry

Open Access Article. Published on 26 March 2026. Downloaded on 4/7/2026 11:06:58 PM.
This article is licensed under a Creative Commons Attribution-NonCommercial 3.0 Unported Licence.

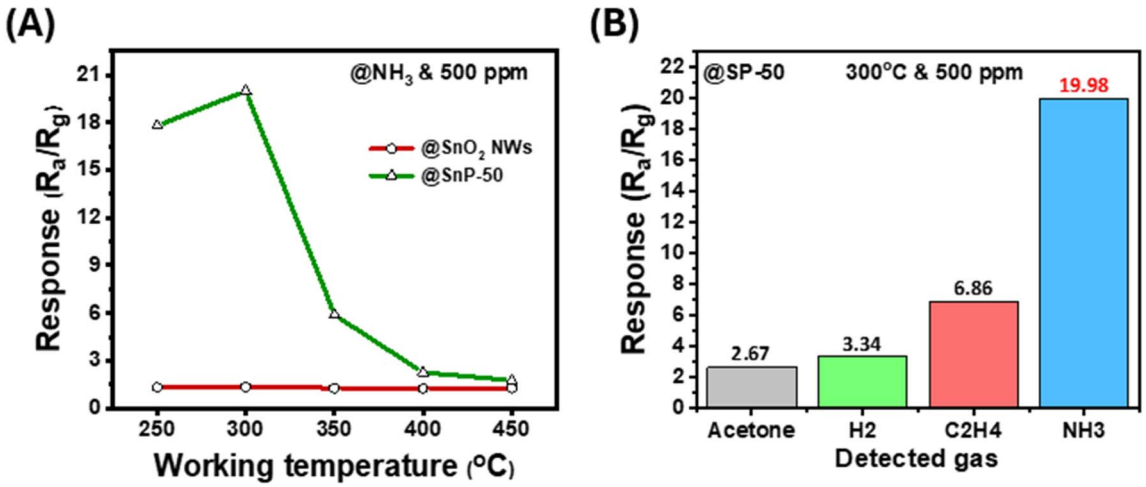

Fig. 8 (A) Comparison of the responses of sensor based on pure-SnO_2 nanowires and PS-50 sensor toward 500 ppm NH_3 at different temperatures and the (B) selectivity of the PS-50 sensor in the presence of contaminant gases.

concentration, and a tendency toward saturation is observed as the NH_3 concentration approaches 500 ppm. In addition, the sensor exhibited the highest response at 300 °C (response value of 19.98 for 500 ppm NH_3), which was identified as the optimal working temperature. The optimal sensing temperature of 300 °C is attributed to the dominant presence of highly reactive chemisorbed O^- species, which promote efficient surface redox reactions with target gas molecules. At lower temperatures, oxygen activation and reaction kinetics are limited, while at higher temperatures, rapid gas desorption reduces the probability of surface reactions and decreases the sensor response.

To demonstrate the enhancement in NH_3 sensing performance after decorating with Pt nanoparticles, the pure-SnO_2 nanowires and Pt-decorated SnO_2 nanowires-based sensors were tested toward 500 ppm NH_3 at 250–450 °C. As illustrated in Fig. 8A, the Pt–SnO_2 nanowire sensor demonstrates significantly higher response values than the pure SnO_2 nanowire sensor across the entire temperature range. In addition, Fig. 8A illustrates an upward trend in the sensor's response with a decrease in temperature from 450 °C to 300 °C. The Pt–SnO_2 nanowire sensor shows the highest response at 300 °C. In contrast, when the temperature decreases to 250 °C, the sensor response declines because, at lower temperatures, the number of active chemisorbed oxygen species (O^-) is reduced and the surface reaction kinetics is slower. Furthermore, the PS-50 sensor showed a 19-fold higher response than the SnO_2 nanowire-based sensor under identical conditions, confirming the significant catalytic role of Pt nanoparticles.

We investigated the selectivity of the PS-50 sensor against the contamination of 500 ppm C_2H_4, H_2 and acetone at the optimal working temperature of 300 °C. The response of the PS-50 sensor to 500 ppm of different gases is plotted in Fig. 8B. The response values were 2.67, 3.34, 6.86 and 19.98 for acetone, H_2, C_2H_4, and NH_3, respectively. Herein, the sensor exhibits the highest response toward NH_3, which may be attributed to the fact that NH_3 is a polar molecule with a lone pair of electrons on the nitrogen atom. This enables strong interaction with the Lewis acid sites (Sn^{4+}) on the SnO_2 surface. In contrast, H_2 is nonpolar, while C_2H_4 and acetone require more complex oxidation mechanisms. Thus, the results demonstrated that the

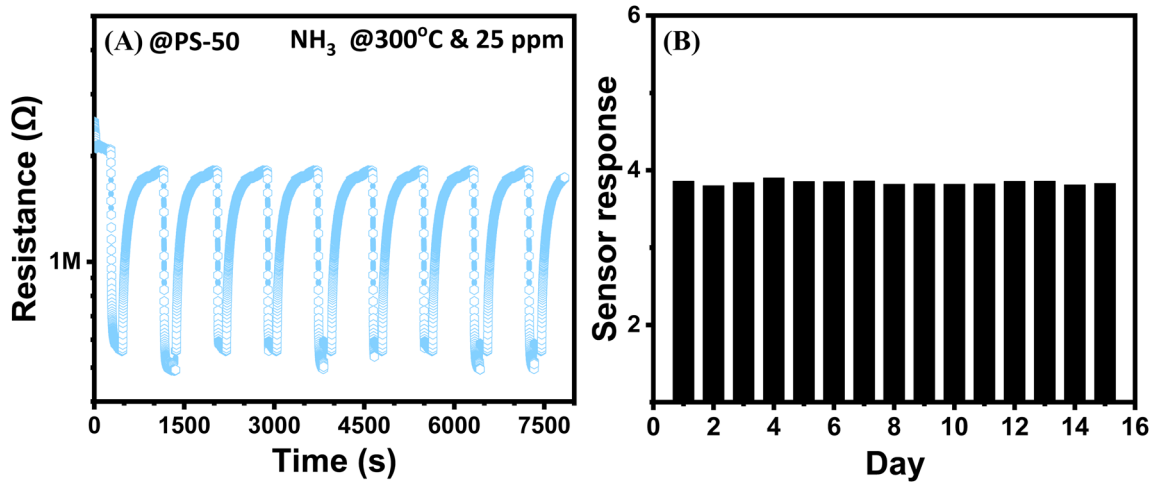

Fig. 9 (A) Short-term stability of PS-50 towards 25 ppm NH_3 and (B) their long-term stability over 15 days.

Open Access Article. Published on 26 March 2026. Downloaded on 4/7/2026 11:06:58 PM. This article is licensed under a Creative Commons Attribution-NonCommercial 3.0 Unported Licence.

Table 2 Comparison of NH_3 gas-sensing performance between the current work and previous reports

Material	Method	Concentration	Response (R_a/R_g)	Temperature	References
PANI/Fe doped CeO_2 nanocomposite	*In situ* polymerisation	25 ppm	500[b]	RT	28
CuO/WO_3	Thermal evaporation and sputtering	100 ppm	673[b]	300	29
$SnO_2/Pt/WO_3$	Sputtering	5 ppm	2.36[a]	250	13
ZnO	CVD	1000 ppm	22.5[b]	300	30
SnO_2/PPy	Hydrothermal	200 ppm	200[b]	RT	31
Pt/SnO_2	Sputtering	450 ppm	25.7[a]	230	32
Pt/SnO_2	CVD and sputtering	500 ppm	20[a]	300	This work

[a] Response defined as R_a/R_g. [b] Response defined as $(R_a - R_g)/R_a \times 100(\%)$.

PS-50 sensor exhibits an excellent selectivity toward NH_3 detection.

The long-term and short-term stability of the PS-50 sensor were studied at 300 °C and the data are shown in Fig. 9. The short-term stability was assessed by repeatedly switching the atmosphere between air and 25 ppm NH_3 for nice pulses. As illustrated in Fig. 9A, the sensor response demonstrated high repeatability over most cycles, and the resistance fully recovered to its baseline value upon exposure to fresh air.

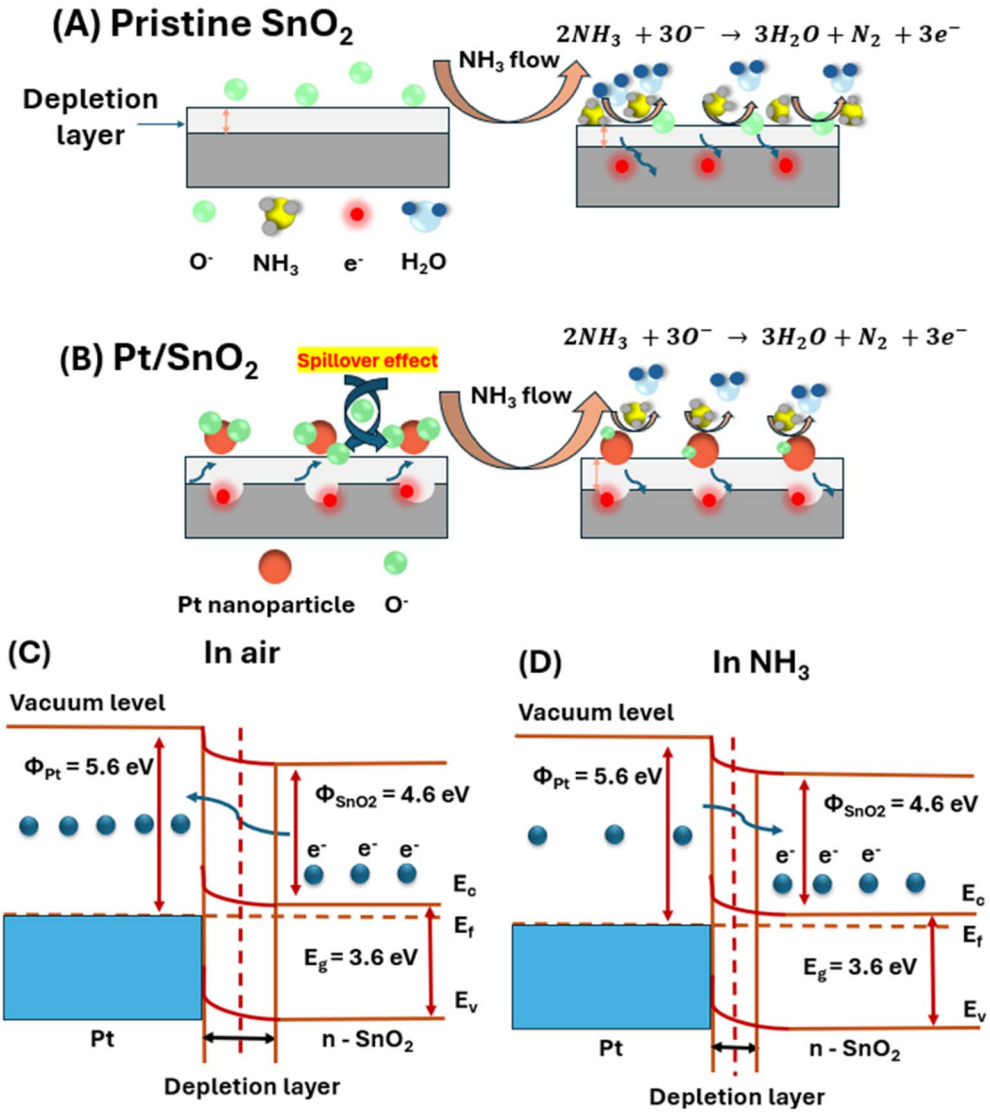

Fig. 10 Schematic of the NH_3 gas-sensing mechanism of (A) pristine SnO_2 and (B) Pt/SnO_2 in the presence of air and NH_3. (C) and (D) Energy band diagram of the PS sensor in the presence of air and NH_3.

© 2026 The Author(s). Published by the Royal Society of Chemistry

Open Access Article. Published on 26 March 2026. Downloaded on 4/7/2026 11:06:58 PM. This article is licensed under a Creative Commons Attribution-NonCommercial 3.0 Unported Licence.

The long-term stability of the sensor was tested for 15 days, and the results reveal the good stability of the sensor with negligible sensor response degradation (Fig. 9B). Nevertheless, the PS-50 sensor exhibited a stable response over the entire experimental period, suggesting its potential for practical applications. The good stability of the sensor was attributed to the high crystallinity of the SnO_2 nanowires, and the effective decoration of Pt nanoparticles without aggregation or oxidation of Pt.[18]

We compared our results with other reports on NH_3 sensors. As summarized in Table 2, our sensor showed higher response than SnO_2/Pt thin film and SnO_2/PPy, but lower than others, regardless of the operating temperature. However, we demonstrated that the PS-50 sensor significantly enhanced the response by 19-fold compared to the pristine SnO_2 sensor.

3.1.2 Gas-sensing mechanisms. The gas-sensing mechanism of SnO_2 nanowires and Pt–SnO_2 nanowire sensors can be explained by the surface depletion model. When measured in air as a reference, oxygen molecules are adsorbed on the metal-oxide surface to form O_2^-, O^-, and O^{2-} species, depending on the operating temperatures. The reaction process can be described by the following equations:[33–35]

$$O_2\ (gas) \rightarrow O_2\ (ads) \quad (1)$$

$$O_2\ (ads) + e- \rightarrow O_2^-\ (ads) \quad (2)$$

$$O_2^-\ (ads) + e- \rightarrow 2O^-\ (ads) \quad (3)$$

$$O- + e^- \rightarrow O^{2-}\ (ads) \quad (4)$$

Adsorbed oxygen species extract electrons from the SnO_2 semiconductor thereby generating an electron depletion layer, Fig. 10A.

The absorbed oxygen species capture electrons from the SnO_2 semiconductor and form an electron depletion layer (Fig. 10A). In the moderate temperature range of 200–300 °C, the predominant oxygen species is O^-. Therefore, upon exposure to NH_3, the reaction between the adsorbed oxygen species and NH_3 molecules occurs according to the following equation:

$$2NH_3 + 3O^-\ (ads) \rightarrow N_2 + 3H_2O + 3e^- \quad (5)$$

According to the obtained results, the PS-50 sensor exhibits an improved gas-sensing response compared to the pure SnO_2 sensor. The enhancement of gas-sensing properties of the Pt/SnO_2 nanowire sensor is explained by (i) the spillover effect and (ii) the formation of a Schottky barrier at the interface between the noble Pt metal and the SnO_2 metal-oxide semiconductor.[13] The catalytic activity of Pt nanoparticles sensitizes the dissociation of oxygen molecules into active oxygen and enhances the pre-adsorbed oxygen species on the surface of SnO_2, the so-called spillover effect. In addition, when Pt is decorated on the SnO_2 surface, electrons are transferred from SnO_2 to Pt because its work function (4.6 eV) is lower than that of Pt (work function 5.6 eV). This phenomenon leads to the formation of the Schottky barrier or an electron depletion layer at the Pt/SnO_2 interface.[13] As a result, the Pt decoration facilitates the adsorption of oxygen on the surface layer of SnO_2 nanowires and increases the base resistance of the sensor. NH_3 gas introduced into the chamber can react with the pre-adsorbed oxygen species, as described in eqn (5). Therefore, the captured electrons are released back into the conduction band of SnO_2. As a result, the width of the depletion layer decreases, and the resistance of the sensor decreases.[32] Here, we defined the sensor response as the ratio of the sensor resistance in air to that in NH_3 gas. Therefore, the high initial resistance in air, induced by the catalytic Pt nanoparticles, significantly enhances the sensor response. Thus, our study documented that by effectively controlling the decoration of Pt nanoparticles on the surface of SnO_2 nanowires, where the correlation between Pt catalytic activity and the sensing performance was optimized, we could develop an excellent NH_3 gas sensor.

4. Conclusion

In this study, we successfully synthesized SnO_2 nanowires and Pt-decorated SnO_2 nanowire-based gas sensors with different sputtering times of Pt for NH_3 detection. The morphology, crystal structure, and electrical and gas sensing properties of the fabricated sensors were investigated. The Pt-decorated SnO_2 nanowire materials with a Pt sputtering time of 50 s (PS-50) exhibited the highest response as compared with others, where the highest response value of 19.98 for 500 ppm NH_3 at 300 °C was achieved. The PS-50 sensor also showed fast response/recovery times of 11/200 seconds and 6/9 seconds at 300 °C and 450 °C, respectively. The Pt–SnO_2 sensor could detect the lowest NH_3 concentration of 25 ppm. In addition, the Pt–SnO_2 sensor exhibited a 19-fold enhancement in response value as compared with that of the bare SnO_2 nanowires. The exceptional high response of the PS-50 sensor to NH_3 was attributed to the synergistic effect of the Schottky junction at the interface of Pt and SnO_2 and the catalytic spillover effect of Pt nanoparticles. Our results showed the potential of the Pt–SnO_2 nanowire sensor for applications in toxic gas detection.

Conflicts of interest

The authors declare that they have no known competing financial interests or personal relationships that could have appeared to influence the work reported in this paper.

Data availability

The authors confirm that the data supporting the findings of this study are available within the article.

Acknowledgements

This work was financially supported by the Hanoi University of Science and Technology under project no. T2024-TĐ-008.

Open Access Article. Published on 26 March 2026. Downloaded on 4/7/2026 11:06:58 PM.
This article is licensed under a Creative Commons Attribution-NonCommercial 3.0 Unported Licence.

References

1 N. Tamaekong, C. Liewhiran, A. Wisitsoraat and S. Phanichphant, *Sensors*, 2010, **10**, 7863–7873.
2 S.-J. Kim, I.-S. Hwang, Y. C. Kang and J.-H. Lee, *Sensors*, 2011, **11**, 10603–10614.
3 I.-C. Chen, S.-S. Lin, T.-J. Lin, C.-L. Hsu, T. J. Hsueh and T.-Y. Shieh, *Sensors*, 2010, **10**, 3057–3072.
4 M. Van Damme, L. Clarisse, S. Whitburn, J. Hadji-Lazaro, D. Hurtmans, C. Clerbaux and P.-F. Coheur, *Nature*, 2018, **564**, 99–103.
5 L. Liu, X. Zhang, W. Xu, X. Liu, Y. Li, J. Wei, M. Gao, J. Bi, X. Lu, Z. Wang and X. Wu, *J. Agric. Food Chem.*, 2020, **68**, 3354–3361.
6 R. Zhang, B. Wang, X. Wang, K. Zeng and C. Guo, *Colloids Surf., A*, 2024, **702**, 135037.
7 S. Li, Y. Yuan, Z. Shang, X. Yin, A. Sampaolo, P. Patimisco, V. Spagnolo, L. Dong and H. Wu, *Photoacoustics*, 2023, **33**, 100557.
8 D. Ripepi, R. Zaffaroni, M. Kolen, J. Middelkoop and F. M. Mulder, *Sustain. Energy Fuels*, 2022, **6**, 1945–1949.
9 L. T. Zegebreal, N. A. Tegegne and F. G. Hone, *Sens. Actuators, A*, 2023, **359**, 114472.
10 D. Zhang, J. Wu, P. Li and Y. Cao, *J. Mater. Chem. A*, 2017, **5**, 20666–20677.
11 D. Wang, D. Zhang, Y. Yang, Q. Mi, J. Zhang and L. Yu, *ACS Nano*, 2021, **15**, 2911–2919.
12 D. Zhou, Z. Kang, X. Liu, W. Yan, H. Cai, J. Xu and D. Zhang, *Sens. Actuators, B*, 2023, **392**, 134072.
13 N. Van Toan, C. M. Hung, N. D. Hoa, N. Van Duy, D. Thi Thanh Le, N. Thi Thu Hoa, N. N. Viet, P. H. Phuoc and N. Van Hieu, *J. Hazard. Mater.*, 2021, **412**, 125181.
14 C. Liu, H. Tai, P. Zhang, Z. Ye, Y. Su and Y. Jiang, *Sens. Actuators, B*, 2017, **246**, 85–95.
15 Q. Li, W. Zeng and Y. Li, *Sens. Actuators, B*, 2022, **359**, 131579.
16 W. Zheng, G. Lu, X. Liu, S. Fan, Y. Hu, N. Pinna and J. Zhang, *Matter*, 2025, **8**, 101914.
17 J. Li, N. Zhao, X. Liu, X. Chang, W. Zheng and J. Zhang, *Nano Lett.*, 2026, **26**, 668–675.
18 Z. Wang, L. Zhu, S. Sun, J. Wang and W. Yan, *Chemosensors*, 2021, **9**, 1–32.
19 S. Sen, A. Nilabh and S. Kundu, *Microchem. J.*, 2021, **165**, 106111.
20 Y. Xu, J. Xie, Y. Zhang, F. Tian, C. Yang, W. Zheng, X. Liu, J. Zhang and N. Pinna, *J. Hazard. Mater.*, 2021, **411**, 125120.
21 Y. Xu, W. Zheng, X. Liu, L. Zhang, L. Zheng, C. Yang, N. Pinna and J. Zhang, *Mater. Horiz.*, 2020, **7**, 1519–1527.
22 J. Shen, F. Li, B. Yin, L. Sun, C. Chen, S. Wen, Y. Chen and S. Ruan, *Sens. Actuators, B*, 2017, **253**, 461–469.
23 (*a*) T. M. Ngoc, N. Van Duy, C. M. Hung, N. D. Hoa, N. N. Trung, H. Nguyen and N. Van Hieu, *RSC Adv.*, 2018, **8**, 36323–36330; (*b*) T. T. N. Hoa, N. V. Duy, C. M. Hung, N. V. Hieu, H. H. Hau and N. D. Hoa, *RSC Adv.*, 2020, **10**, 17713–17723.
24 N. Van Hieu, L. T. B. Thuy and N. D. Chien, *Sens. Actuators, B*, 2008, **129**, 888–895.
25 D. T. T. Le, S. Iannotta, N. V. Hieu, C. Corradi, T. Q. Huy, M. Pola and M. Tonezzer, *J. Nanosci. Nanotechnol.*, 2014, **14**, 5088–5094.
26 S. Wang, L. Sang, Z. Jiao, F. Zhang, K. Wang, B. Xu, P. Zhang, B. Liu, Y. Wang, Y. Li and R. Hu, *Appl. Surf. Sci.*, 2025, **687**, 162257.
27 S. H. S. Pai, A. Mondal, R. Barathy T, B. Ajitha, J. J. Samuel E and Y. A. K. Reddy, *Int. J. Hydrogen Energy*, 2024, **50**, 928–941.
28 C. Esmaeili, S. Ashtiani, C. Regmi, A. Laposa, J. Voves, J. Kroutil, K. Friess, V. Povolny and S. Lotfian, *Heliyon*, 2024, **10**, 0–11.
29 S. Park, S. Park, J. Jung, T. Hong, S. Lee, H. W. Kim and C. Lee, *Ceram. Int.*, 2014, **40**, 11051–11056.
30 S. J. Chang, W. Y. Weng, C. L. Hsu and T. J. Hsueh, *Nano Commun. Netw.*, 2010, **1**, 283–288.
31 Y. Li, H. Ban and M. Yang, *Sens. Actuators, B*, 2016, **224**, 449–457.
32 M. Shahabuddin, A. Sharma, J. Kumar, M. Tomar, A. Umar and V. Gupta, *Sens. Actuators, B*, 2014, **194**, 410–418.
33 Y. Masuda, *Sens. Actuators, B*, 2022, **364**, 131876.
34 N. V. Toan, C. M. Hung, N. D. Hoa, N. V. Duy, D. T. T. Le, N. T. T. Hoa, N. N. Viet, P. H. Phuoc and N. V. Hieu, *J. Hazard. Mater.*, 2021, **412**, 125181.
35 N. P. Hung, N. V. Duy, C. T. Xuan, D. T. T. Le, C. M. Hung, H. Jin and N. D. Hoa, *RSC Adv.*, 2024, **14**, 12438–12448.

© 2026 The Author(s). Published by the Royal Society of Chemistry